TCAD accurate modeling of trap-induced effects in GaN HEMTs

TCAD accurate modeling of trap-induced effects in GaN HEMTs

Simona Donati Guerrieri, Eva Catoggio, Fabrizio Bonani

Dept. Electronics and Telecommunications, Politecnico di Torino, Torino, Italy
simona.donati@polito.it

***Abstract*—In this work we demonstrate an accurate Technology Computer Aided Design (TCAD) modeling approach for the analysis of trap effects on the electrical features of AlGaN/GaN HEMT devices for microwave applications. The physical device model includes the discretized coupled drift -diffusion and trap rate equations system, implemented into an in-house mixed-mode TCAD simulator, and solved in dynamic conditions with the Harmonic Balance (HB) algorithm. The TCAD allows a seamless assessment of the DC, small-signal AC and periodic large-signal (LS) behavior of GaN HEMTs as a function of the trap properties. A test-case addresses the analysis of 29 GHz class B power amplifier based on a Fe-doped 150 nm GaN HEMT as a function of the Fe trap energy, showing that, despite a marked signature on the AC parameters dispersion, traps have a mild impact on single-tone LS behavior even in strongly non-linear operation.**

***Index Terms*—GaN HEMTs; nonlinear device models; TCAD simulations; trap rate equations; DC, AC and large-signal parameters**

I. Introduction

Currently, relatively mature commercial 150 nm gate-length AlGaN/GaN HEMT technologies (see [1]–[3] for SiC-based devices, [4] for Si substrate) are available, with a variety of products covering applications for microwave power up to 40 GHz, including space, satcom, radars and base transceiver stations for 5G. Technology covers the entire range between die-level FETs and full MMIC amplifiers and circuits, however reliability, cost and material quality still need to improve. In particular, the presence of traps and defects [5], [6], both in the bulk and at interfaces, is a technological issue still to be solved.

According to [7]–[10], a main responsible for the device low-frequency dispersion is the buffer doping with C or Fe atoms to reduce the layer conductivity. These dopants surely act as traps, which slow dynamic behavior is responsible for dispersion, but the details of their behavior is greatly debated, since literature shows a wide spread of reported values both for the exact trap energy location and for the electron and hole lifetimes.

This uncertainty calls for the development of accurate and physically sound models to assist the extraction of trap parameters. TCAD simulations play a major role in the identification of GaN traps [11], as providing a direct connection between the spatially distributed traps and the device terminal features. Traditionally, TCAD simulations are limited to time-domain solutions [12], [13], while frequency-domain approaches are much less exploited [14] and, in the vast majority of cases, limited to small-signal analysis. Hence, a unique environment allowing for the seamless analysis from DC to LS operation and the mixed-mode simulation of microwave circuits in the frequency domain is still missing.

In this contribution, we discuss a novel TCAD tool, implementing the drift-diffusion model self-consistently coupled to the dynamic trap rate equations, solved in the frequency domain by means of the Harmonic Balance formulation. The simulator implements a mixed-mode device analysis in LS periodic and quasi-periodic conditions. To demonstrate the TCAD capability we address a 29 GHz class B power amplifier analysis, based on a 150 nm GaN HEMT.

II. The physical model

The physical model is implemented into an in-house TCAD tool where the two-dimensional drift-diffusion model is solved coupled to a trap rate equation for each considered trap:

$$\nabla\cdot(\epsilon\nabla\varphi) = -q\cdot\left(p-n+N_D-N_A-\sum_k n_{T,k}\right.$$
$$\left.+\sum_k \delta_k N_{T,k}\right) \tag{1}$$

$$\frac{\partial n}{\partial t} = \frac{1}{q}\nabla\cdot\mathbf{J}_n - \sum_k (R_{n,k}-G_{n,k}) \tag{2}$$

$$\frac{\partial p}{\partial t} = -\frac{1}{q}\nabla\cdot\mathbf{J}_p - \sum_k (R_{p,k}-G_{p,k}) \tag{3}$$

$$\frac{\partial n_{T,k}}{\partial t} = (R_{n,k}-G_{n,k}) - (R_{p,k}-G_{p,k}) \tag{4}$$

where φ is the electrostatic potential, n, p the electron and hole densities, $\mathbf{J}_{\{n,p\}}$ the drift-diffusion current density, and N_D and N_A the ionized doping concentrations. $N_{T,k}$ represents the total concentration of the k-th trap, while $n_{T,k}$ is the corresponding concentration of occupied traps. Finally, q is the elementary charge and ϵ the material permittivity. The Kronecker δ_k is 0 for acceptor-like traps and 1 for donor traps. $R_{\{n,p\},k}$ and $G_{\{n,p\},k}$ are the recombination and generation rates due to the electron and hole trap mechanism for the k-th trap, expressed according to the Shockley-Read-Hall formulation [14]. Traps are considered non interacting in terms of energy transitions and with local trap rate equations.

From a numerical standpoint, the model equations (1)-(4) are discretized and converted into a system of algebraic equations compactly expressed as

$$\mathbf{D}^{(\alpha)}\dot{\mathbf{x}} = \mathbf{F}^{(\alpha)}(\mathbf{x}, \mathbf{e}; \boldsymbol{\sigma}) \qquad \alpha = \varphi, n, p, n_T \tag{5}$$

where $\alpha = \varphi$ refers to the Poisson equation (1), $\alpha = n, p$ to the electron and hole continuity equations (2)-(3), and $\alpha = n_T$ to the trap rate equation (4) (we consider here $k = 1$ for simplicity). Vector $\boldsymbol{\sigma}$ represents the collection of the model parameters such as e.g. trap energy, cross section, total concentration. Vector $\mathbf{x}$ collects the nodal values of the system unknowns, while $\mathbf{e}$ represents the set of the external electrical generators applied to device contacts. $\mathbf{D}^{(\alpha)}$ is a diagonal matrix accounting for the system memory through the time-derivatives $\dot{\mathbf{x}}$, while $\mathbf{F}$ is the memory-less part [15]. For transient TCAD analysis, (5) is further discretized in the time domain and solved with generic time-varying sources $\mathbf{e}$. However, with periodic external sources, frequency domain analysis through Harmonic Balance (HB) is better suited to describe the device. In TCAD HB analysis, the external sources $\mathbf{e}$ correspond to the superposition of DC plus harmonic stimuli with fundamental frequency ω_0, thereby forcing the device in periodic large-signal operation. System (5) is converted into the frequency domain yielding the HB system [15]

$$\mathbf{D}^{(\alpha)}\boldsymbol{\Omega}\mathbf{X} = \boldsymbol{\Gamma}\mathbf{F}^{(\alpha)}(\boldsymbol{\Gamma}^{-1}\mathbf{X}, \mathbf{E}; \boldsymbol{\sigma}) \qquad \alpha = \varphi, n, p, n_T \tag{6}$$

where $\mathbf{X}$ and $\mathbf{E}$ are the collection of the harmonic amplitudes of $\mathbf{x}(t)$ and $\mathbf{e}(t)$, respectively. $\boldsymbol{\Omega}$ is an operator representing time derivation in the frequency domain, and $\boldsymbol{\Gamma}^{-1}$ is the operator implementing the discrete Fourier transform.

III. Example

To demonstrate the capability of the developed software for a comprehensive LS analysis of GaN HEMTs, we address the simulation of a AlGaN/GaN HEMT from the 150 nm technology, whose cross section is reported in Fig. 1. The polarization charge was calculated with the models presented in [14], the Al model fraction is 25% and the polarization charge activation is 90%. The device is characterized by a buffer deep acceptor Fe doping with a concentration $N_\mathrm{T} = 10^{18}$ cm^{-3}, and energy $E_\mathrm{T} = E_\mathrm{C} - \Delta E_\mathrm{T}$ (i.e., ΔE_T below the conduction band). The deep acceptor acts as a trap with electron and hole capture cross-sections $\sigma_n = \sigma_p = 3 \times 10^{-16}$ cm^2, inducing a low-frequency dynamics. All the other charges (residual donor $N_\mathrm{D} = 10^{15}$ cm^{-3} doping and superficial charge $\sigma_\mathrm{int}/q = -2 \times 10^{12}$ cm^{-2} at the passivation interface) are considered as fixed. Here we present the simulation results varying the trap level, namely $\Delta E_\mathrm{T} = [0.3, 0.4, 0.5]$ eV.

DC simulations are carried out with the three energy levels, showing that increasing trap distance from the conduction band, the number of trapped electrons increases and the drain current reduces. As a result, the saturation drain current is reduced while the threshold voltage increases. Partial results of the DC simulation campaign are reported in Fig. 2 (output characteristics at $V_G = 0$, i.e. the saturation current) and Fig. 3 (transcharacteristic at $V_D = 10$ V). The threshold ranges from $V_\mathrm{T} = -2.1$ V to $V_\mathrm{T} = -1.9$ V.

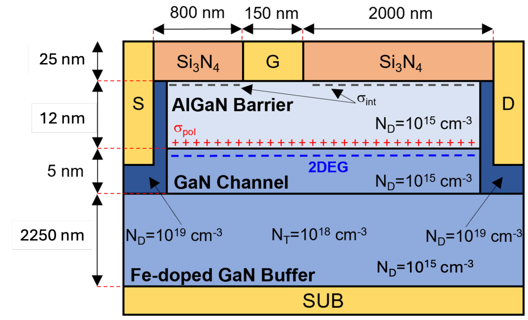

Fig. 1. Cross-section of the analysed structure.

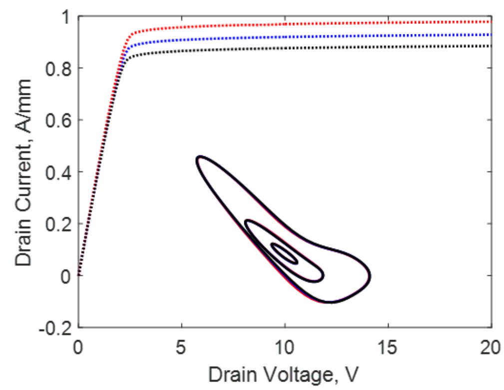

Fig. 2. DC (dashed) and dynamic (solid) drain current in the output characteristic plane and varying trap energy. Red: $\Delta_{E_\mathrm{T}} = 0.3$ eV ; blue: $\Delta_{E_\mathrm{T}} = 0.4$ eV; black: $\Delta_{E_\mathrm{T}} = 0.5$ eV. The operating frequency is 29 GHz. The three dynamic curves correspond to input available power of 5, 15 and 22.5 dBm.

Focusing on a possible application of a near class B power amplifier, we carry out AC and LS simulations with the three selected trap energy levels. To make the results comparable, despite the different DC behavior, we select the bias point with a gate bias voltage that ensures the same DC bias current $I_{D0} = 85$ mA ($\approx 10\%$ I_DSS). This effectively corresponds to the same gate overdrive. The drain voltage is set to $V_D = 10$ V.

AC simulations are reported with frequency ranging from 1 kHz to 10 GHz. The output conductance is the parameter where the trap dynamic induces significant frequency dispersion both in the real and the imaginary parts. These are reported in Figures 4 and 5. As expected [16], the real part shows an increasing trend of the Y_{22} element of the AC Y matrix, associated with the well known degradation of the output resistance and the increased power loss of power amplifiers in dynamic conditions with respect to quasi-static operation. Correspondingly, the imaginary parts exhibits a clear peak in the lower frequency range. The trap energy determines the peak frequency (imaginary part) or the transition frequency (real part) which ranges from less than 1 KHz to 750 kHz. At microwave frequencies, the three devices become identical since the traps are entirely frozen.

Turning to the LS case, we carry out an analysis akin to a class B amplifier with tuned load at 29 GHz. The device gate

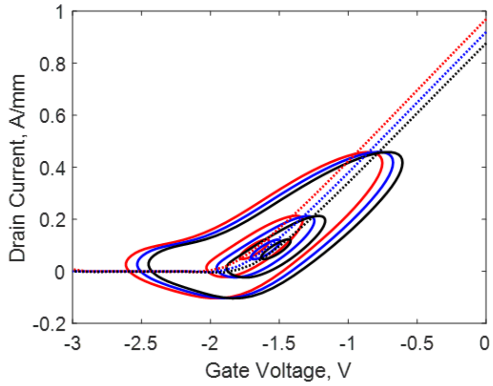

Fig. 3. DC (dashed) and dynamic (solid) drain current in the transcharacteristic plane. Red: $\Delta_{E_\mathrm{T}} = 0.3$ eV ; blue: $\Delta_{E_\mathrm{T}} = 0.4$ eV; black: $\Delta_{E_\mathrm{T}} = 0.5$ eV. The operating frequency is 29 GHz. The three dynamic curves correspond to input available power of 5, 15 and 22.5 dBm.

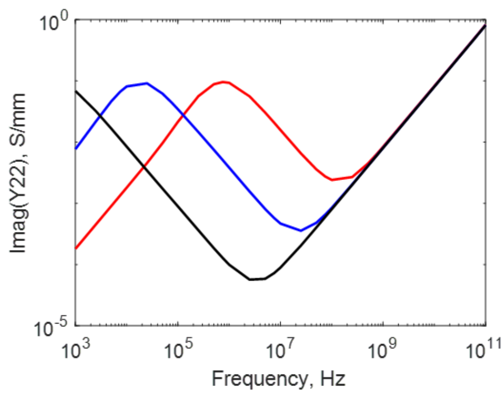

Fig. 4. Imaginary part of the Y22 element of the admittance matrix. Same color notation as previous figures.

periphery is 1 mm. In this preliminary analysis the fundamental load $Z_\mathrm{L} = (15 + j6)\ \Omega$ has been extracted from a simplified approach rather than from load-pull simulations. The real part is calculated with the load line approach. The imaginary part is calculated to tune out the device output capacitance at the operating frequency. Figures. 2 and 3 show the dynamic load lines at three input powers showing significant LS distortion. As expected the three curves are nearly identical when reported in the output characteristic plane (Fig. 2), while the different choice of the gate bias voltage is clearly seen when reported in the transfer characteristic case (Fig. 3). Some difference in the dynamic behavior can be observed at higher input power, where the nonlinearities start to play the major role and, in particular, when a significant self-bias is present. Concerning the power performance, Fig. 6 shows the transducer gain as a function of the input power. The gain compression is already close to 1 dB in the analyzed power range. Turning to trap dispersion, it is interesting to analyze if self-bias can be affected by the trap low frequency behavior. As reported in Fig. 7 the simulations suggest that traps play a limited role, since the three analysed cases behave quite similarly.

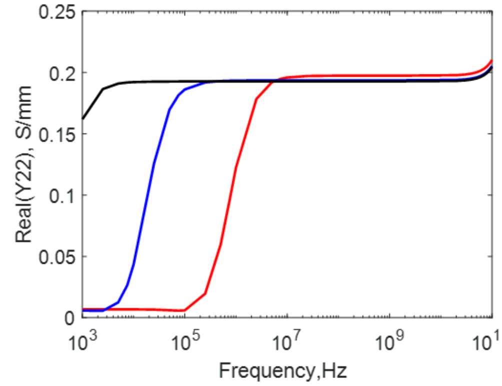

Fig. 5. Real part of the Y22 element of the admittance matrix. Same color notation as previous figures.

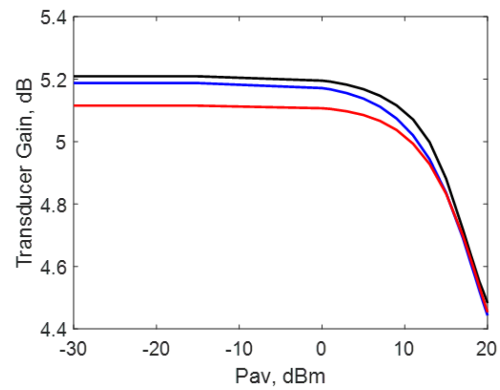

Fig. 6. Transducer gain as a function of the available input power. Same color notation as previous figures.

IV. Conclusion

We presented a comprehensive environment to simulated HEMT devices even in presence of trap dynamics. Despite traps insert distinctive frequency coloring in the AC parameters, they play a limited role in single frequency LS operation,

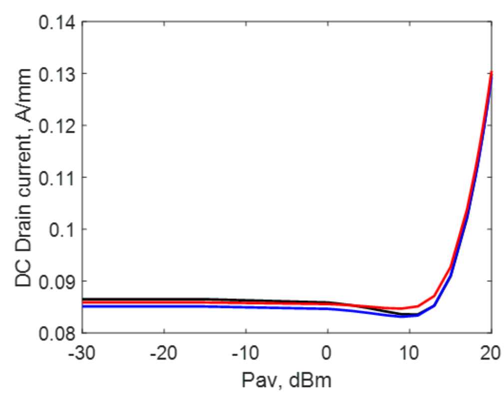

Fig. 7. DC component of the drain current under LS operation as a function of the available input power. Same color notation as previous figures.

even in presence of harsh nonlinearities induced by the class B operation. More investigation will be carried out using multitone inputs and with harsh compression. Additionally, the TCAD software allows for a seamless temperature-dependent trap analysis [17].

REFERENCES

[1] "UMS GaN GH15-10," https://www.ums-rf.com/ums-gan-gh15-10-technology-is-space-evaluated/.

[2] "The Qorvo GaN advantage," https://www.qorvo.com/innovation/technology/gan.

[3] "MMIC advanced technology," https://www.winfoundry.com/en-US/Tech/tech_advanced.

[4] "III – V processes," https://www.ommic.com/iii-v-processes/.

[5] K. Wang, H. Jiang, Y. Liao, Y. Xu, F. Yan, and X. Ji, "Degradation prediction of GaN HEMTs under hot-electron stress based on ML-TCAD approach," *Electronics*, vol. 11, no. 21, p. 3582, Nov. 2022.

[6] N. Modolo, C. D. Santi, A. Minetto, L. Sayadi, G. Prechtl, G. Meneghesso, E. Zanoni, and M. Meneghini, "Trap-state mapping to model GaN transistors dynamic performance," *Scientific Reports*, vol. 12, no. 1, Feb. 2022.

[7] V. Joshi, A. Soni, S. P. Tiwari, and M. Shrivastava, "A comprehensive computational modeling approach for AlGaN/GaN HEMTs," *IEEE Transactions on Nanotechnology*, vol. 15, no. 6, pp. 947–955, Nov. 2016.

[8] S. Cangini, G. P. Gibiino, A. M. Angelotti, C. Florian, A. Santarelli, and M. Lorenzini, "Experimental characterization of drain current transient effects in 'buffer-free' RF GaN HEMTs," in *2024 15th German Microwave Conference (GeMiC)*. IEEE, Mar. 2024, pp. 33–36.

[9] H. Yu, B. Parvais, U. Peralagu, R. Y. ElKashlan, R. Rodriguez, A. Khaled, S. Yadav, A. Alian, M. Zhao, N. De Almeida Braga, J. Cobb, J. Fang, P. Cardinael, A. Sibaja-Hernandez, and N. Collaert, "Back barrier trapping induced resistance dispersion in GaN HEMT: Mechanism, modeling, and solutions," in *2022 International Electron Devices Meeting (IEDM)*, vol. 58. IEEE, Dec. 2022, pp. 30.6.1–30.6.4.

[10] K. Li, T. Matsuda, E. Yagyu, K. H. Teo, and S. Rakheja, "Trapping phenomena in GaN HEMTs with Fe- and C-doped buffer," in *2022 Device Research Conference (DRC)*. IEEE, Jun. 2022, pp. 1–2.

[11] N. K. Subramani, "Physics-based tcad device simulations and measurements of gan hemt technology for rf power amplifier applications, phd dissertation, university of limoges, 2017." 2017, https://tel.archives-ouvertes.fr/tel-01702325. [Online]. Available: https://tel.archives-ouvertes.fr/tel-01702325

[12] G. Meneghesso, G. Verzellesi, F. Danesin, F. Rampazzo, F. Zanon, A. Tazzoli, M. Meneghini, and E. Zanoni, "Reliability of GaN high-electron-mobility transistors: State of the art and perspectives," *IEEE Transactions on Device and Materials Reliability*, vol. 8, no. 2, pp. 332–343, Jun. 2008.

[13] N. Zagni, G. Verzellesi, and A. Chini, "Temperature-independent current dispersion in 0.15 μm AlGaN/GaN HEMTs for 5G applications," *Micromachines*, vol. 13, no. 12, p. 2244, Dec 2022.

[14] E. Catoggio, S. Donati Guerrieri, and F. Bonani, "TCAD modeling of GaN HEMT output admittance dispersion through trap rate equation Green's functions," *Electronics*, vol. 12, no. 11, p. 2457, May 2023.

[15] F. Bonani, S. Donati Guerrieri, G. Ghione, and M. Pirola, "A TCAD approach to the physics-based modeling of frequency conversion and noise in semiconductor devices under large-signal forced operation," *IEEE Transactions on Electron Devices*, vol. 48, no. 5, pp. 966–977, May 2001.

[16] E. Catoggio, S. D. Guerrieri, and F. Bonani, "TCAD analysis of GaN HEMT AC parameters through accurate solution of trap rate equations," in *2023 18th European Microwave Integrated Circuits Conference (EuMIC)*. IEEE, Sep. 2023, pp. 33–36.

[17] E. Catoggio, S. Donati Guerrieri, and F. Bonani, "Efficient TCAD thermal analysis of semiconductor devices," *IEEE Transactions on Electron Devices*, 2021.